International Communications in Heat and Mass Transfer 116 (2020) 104644

Contents lists available at ScienceDirect

International Communications in Heat and Mass Transfer

journal homepage: www.elsevier.com/locate/ichmt

# Experimental and numerical investigation on flow and heat transfer of impingement jet cooling of kerosene

Mengmeng Du[a,b], Fengquan Zhong[a,b,*], Yunfei Xing[a], Xinyu Zhang[a,b]

[a] State Key Laboratory of High Temperature Gas Dynamics, Institute of Mechanics, Chinese Academy of Sciences, Beijing 100190, China
[b] School of Engineering Science, University of Chinese Academy of Sciences, Beijing 100049, China

ARTICLE INFO

*Keywords:*
Impingement jets
Kerosene
Heat transfer coefficient
Pressure loss
Reynolds number

ABSTRACT

In this study, flow and convective heat transfer of multiple impingement jets of kerosene are investigated experimentally and numerically. A test panel with multiple impingement holes is used to perform experimental study with a heating facility. The overall heat transfer coefficient and pressure loss are measured for a wide Reynolds number range of impingement jets from 2020 to 14,260. For the present flow parameters range, Nusselt number of kerosene impingement jet cooling is found to vary with a function of Reynolds number of $Re^{0.7}$. The pressure loss coefficient decreases with the increase of Reynolds number with a function of $Re^{-0.48}$. At the same time, Reynolds averaged numerical method with SST k-ω turbulence model is applied to simulate flow field and heat transfer of impingement jet cooling. The calculated heat transfer coefficient and pressure loss are well consistent with the experimental data. The numerical results clearly show the high-speed jets and strong vortices near the impingement plate cause high heat transfer efficiency.

## 1. Introduction

Impinging jet flow has prominent heat transfer efficiency and it has been broadly applied in many engineering fields for heat exchange or cooling [1–3]. Its flow and heat transfer properties are related to many of geometrical parameters including impingement hole size, hole-to-hole distance and arrays, impingement height as well as flow parameters such as inlet flow velocity, temperature and Reynolds number. Garimella and Rice [4] experimentally studied heat transfer of liquid FC-77 of single circular impingement jet and heat transfer correlations were proposed for the averaged Nusselt number as functions of Reynolds number, Prandlt number, impingement height and hole size. Huber and Viskanta [5] studied effects of hole-to-hole distance on heat transfer coefficient of air impingement jets, and their experimental results indicated that there exist strong jets interactions, affecting heat transfer efficiency. San and Chen [6] experimentally investigated combined effects of impingement height and jet-to-jet spacing on heat transfer features of air impinging jet. Sparrow and Lovell [7] experimentally studied the heat transfer properties of oblique impinging jet. Their results indicated that the location of peak in heat transfer coefficient was offset from the stagnation points of the impingement jets. Bizzak and Chyu [8] studied the secondary peak of heat transfer coefficient for air impingement jet utilizing laser-induced fluorescence thermal imaging system. Li and Garimella [9] studied experimentally heat transfer properties of impingement jet with different coolants incuding gases and liquids, and the effects of Prandtl number on heat transfer of impinging jet was discussed. Xing et al. [10] performed an experimental and numerical investigation on heat transfer of air impingement jet. The visualization and measurement of heat transfer coefficient on the impingement plate is accomplished by transient liquid crystals method. Yu [11] studied effect of pin fin configurations on heat transfer efficiency of air impingement jet flow. Vinze et al. [12] studied the effect of dimple on heat transfer of air impingement jets. Their results indicated that structures of pin fin or dimple on the impingement wall can further increase heat transfer ability. It is worthy noticing that majority of the previous studies concentrated on impingement jet flow of simple liquids such as air or water etc. Research works on impingement heat transfer of hydrocarbon fuels, for example, aviation kerosene, are very few. It is known that aviation kerosene has been used as an effective coolant of active cooling system for aerospace engine applications [13,14]. Compared to simple liquids, kerosene is a fuel mixture comprised of many hydrocarbon species and it behaves complicated changes in transport and thermodynamic properties [15,16]. To the authors' knowledge, so far, flow and heat transfer properties of impingement jet with aviation kerosene have not been well studied yet. Since hydrocarbon fuels are considered as good coolant candidates for thermal protection of aero-engines, impingement jet cooling of hydrocarbon fuels is a very efficient way to increase the

* Corresponding author at: State Key Laboratory of High Temperature Gas Dynamics, Institute of Mechanics, Chinese Academy of Sciences, Beijing 100190, China.
*E-mail address:* fzhong@imech.ac.cn (F. Zhong).

https://doi.org/10.1016/j.icheatmasstransfer.2020.104644

Available online 03 July 2020

**Nomenclature**

| | |
|---|---|
| $A$ | Area of the impingement surface |
| $Cp$ | Specific heat |
| $d$ | Diameter of impingement jet holes |
| $h$ | Heat transfer coefficient |
| $H$ | Impingement height |
| $k$ | Turbulent kinetic energy |
| $\dot{m}$ | Mass flow rate |
| $Nu$ | Nusselt number |
| $P_f$ | Pressure |
| $Pr$ | Prandtl number |
| $q_w$ | Wall heat flux |
| $Re$ | Reynolds number |
| $T_1$ | Fuel temperature at the inlet |
| $T_2$ | Fuel temperature at the outlet |
| $T_f$ | Averaged fuel temperature |
| $T_w$ | Wall temperature |
| $U$ | Jet velocity |
| *Greek symbols* | |
| $\delta_j$ | Thickness of the orifice plate |
| $\Delta P$ | Pressure loss |
| $\lambda$ | Thermal conductivity |
| $\mu$ | Dynamic viscosity |
| $\xi$ | Pressure loss coefficient |
| $\rho$ | Density |

overall cooling effectiveness. Therefore, it is significant to investigate flow and heat transfer characteristic of aviation kerosene impingement jets and to examine cooling efficiency of impingement jet flow of kerosene.

In the current work, flow and heat transfer features of kerosene through a multiple impingement holes plate with varied inlet flow parameters are investigated experimentally and numerically. The measurements of heat transfer coefficient and pressure loss for different experimental parameters are obtained and their correlations as functions of Reynolds number and Prandtl number are developed. Kerosene impingement jet flow at two typical flow conditions are then numerically simulated and detail results of flow configuration and heat transfer distribution are presented.

## 2. Experimental apparatus

A schematic diagram of the experimental facility is illustrated in Fig. 1. The heating facility is consist of a fuel tank with a gas driven system, a fuel pre-heater, a test section with a mica heating system and a collecting system downstream of the test section. Measurements of pressure, temperature, mass flow rate are provided with a data acquisition system. More detailed description about the facility are given in our previous works [17,18].

The test panel with impingement holes is heated via mica heater with DC power supply. During the experiments, the test panel is well insulated with Alumina-Silicate refractory fiber layer. As shown in Fig. 2(a), the test panel has a orifice plate with a thickness $\delta_j$ of 3 mm to generate high-speed jet flow to impinge on the target plate with thermal loadings. The orifice plate has four jet holes with a diameter $d$ of 1 mm are evenly distributed on the plate. The hole-to-hole horizontal distance is 16 mm and the longitudinal distance is 12 mm as indicated in Fig. 2(b). The distance from the orifice plate to the impingement surface as called as impingement height H, is 3 mm. The cavity between the orifice plate and the impingement surface provides a space for develoepment and interaction of impingement jet flow. As shown in Fig. 2(a), kerosene flows into the collecting groove from the inlet, and then goes through the orifice plate to form high-speed jets under pressure differences. The kerosene jets hit the impingement surface and result in significant convective heat transfer. Finally, the kerosene leaves the test panel through the outlet pipe. After each experiment, nitrogen is driven into the test section to clean the system and to prevent coke deposition.

K-type thermocouples are mounted at the inlet and the outlet to record the increase of kerosene temperature. A differential pressure transducer with high accuracy is used to measure the pressure difference of keroene flow between the inlet and the outlet. There are two K-type thermocouples spot-welded on the outer surface of the target plate of the test panel to obtain the time change of wall temperatures under heating and impingement jet cooling. A Coriolis flowmeter is used to measure mass flow rate and a pressure sensor is utilized to obtain the fuel pressure at the inlet.

## 3. Data analysis

Kerosene flow absorbs heat from the impingement surface and its temperature increases at the outlet of the test panel. Therefore, based on the energy conservation law, the average wall heat flux $q_w$ through

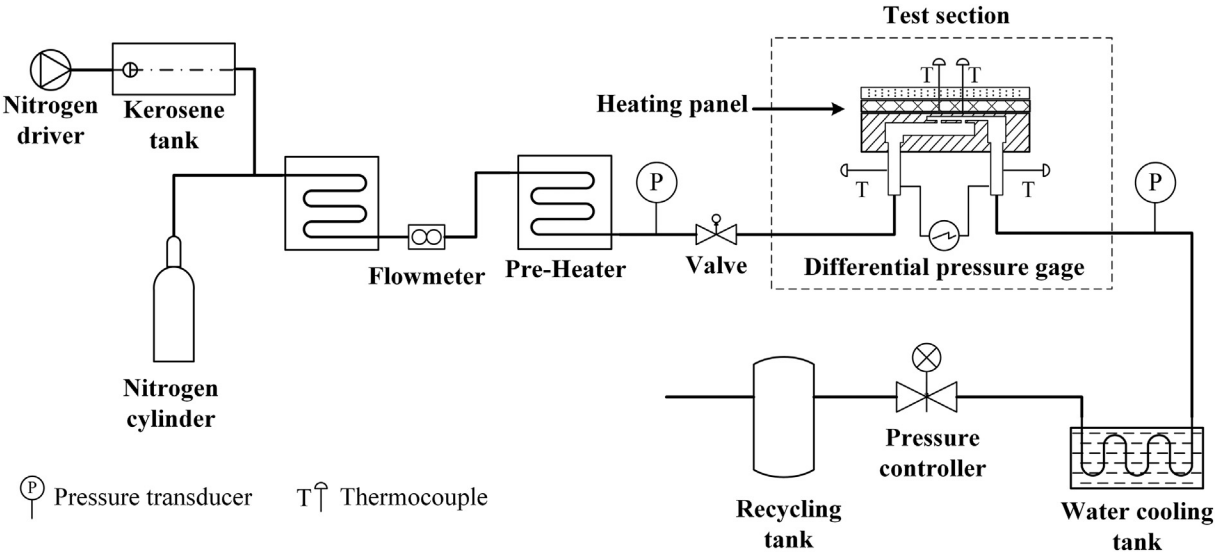


**Fig. 1.** Shematic diagram of the experimental setup.

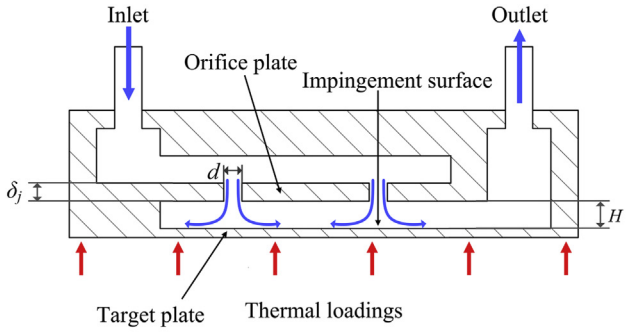


(a) Test panel

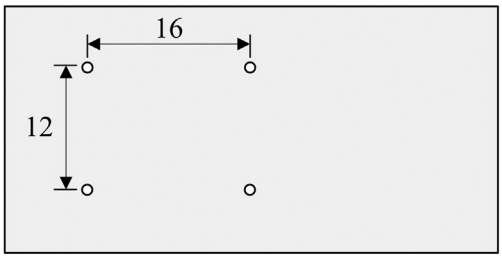


(b) Distribution of impingement holes (unit: mm)

**Fig. 2.** Schematic diagram of the test section.

the impingement surface can be determined by the measured inlet and outlet temperatures as calculated as follows:

$$q_w = \frac{\dot{m}}{A}\int_{T_1}^{T_2} C_p dT \tag{1}$$

where, the upper and lower values of the intergral are fuel temperature at the outlet and the inlet respectively. $C_p$ is specfic heat of kerosene at constant pressure, which is in connection with temperature and pressure and it can be caculated by a 10-species surrogate model proposed in our prior work [16]. $\dot{m}$ is the kerosene mass flow rate, and $A$ is the area of the impinement surface.

The average heat transfer coefficient $h$ on the impingement surface can be caculated by the following equation:

$$h = \frac{q_w}{T_w - T_f} \tag{2}$$

where, $T_f$ is the average kerosene temperature based on the two fuel temperatures measured at the inlet and the outlet. $T_w$ is the wall temperature on the impingement surface and it is determined by the averaged value of the measured wall temperatures with a small temperature difference across the target plate thickness based on one-dimesnional heat conduction relation.

The non-dimensional heat transfer coefficient, Nusselt number ($Nu$) is calculated by:

$$\mathrm{Nu} = \frac{hd}{\lambda} \tag{3}$$

where, λ is the thermal conductivity of kerosene, and $d$ is the diameter of the jet holes.

The pressure loss coefficient is given by:

$$\xi = \frac{\Delta P}{1/2\rho u^2} = \frac{2\pi^2 d^4 \rho \Delta P}{\dot{m}^2} \tag{4}$$

Where $\Delta P$ is the measured pressure difference between the inlet and the outlet. ρ is the density determined by the average kerosene temperature $T_f$ and pressure $P_f$. $u$ is the jet velocity of kerosene across the holes determined by the mass coversation equation.

The jet Reynolds number $Re$ is expressed as $Re = \frac{\rho u d}{\mu}$, where $\mu$ is the viscosity of kerosene.

All the thermophysical parameters of kerosene used in the above equations are determined with a 10-species surrogate of kerosene as described in our prior work [16]. The change of thermal properties of kerosene as a function of temperature at a pressure of 3 MPa are shown in Fig. 3. As shown in the figure, as temperture increases from 300 K to 600 K, density and thermal conductivity decrease by more than 30%. Viscoity of kerosene decreases more considerably with one order in magnitude. At the same time, specific heat rises from 2 kJ/(kg·K) to 3.1 kJ/(kg·K). It is obvious that thermodynamic and transport properties of fuel change significantly in the temperature range of 300 K and 600 K.

For the present measurement data, the uncertainties are determined by calibration results of the measurement transducers including differential pressure transducer, thermocouple and mass flow meter. The thermocouples have a measurement error of 2.1 K, the differential pressure transducer has an error of 0.1% and the uncertainty of mass flow rate is 0.2%. The uncertainties of heat transfer coefficient $h$ and pressure loss coefficient $\xi$ are then calculated by the error propagation formula as described in the literature [19]. The maximum relative

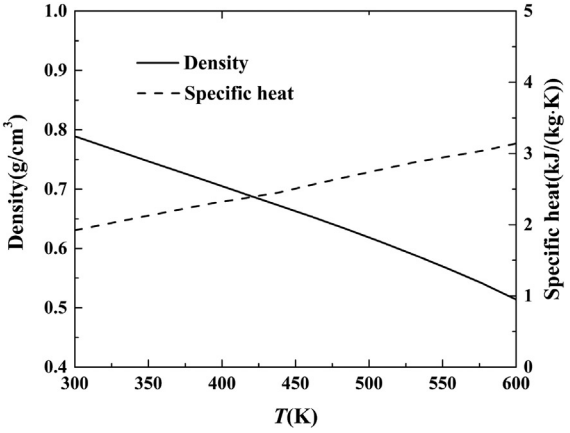


(a) Density and Specific heat

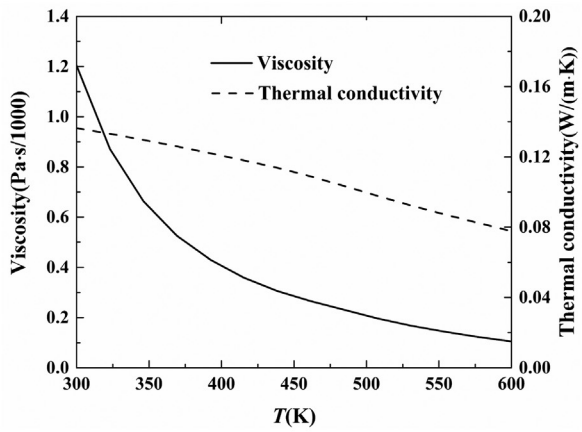


(b) Viscosity and thermal conductivity

**Fig. 3.** Properties of kerosene at 3 MPa.

uncertainty of heat transfer coefficient $h$ is 6.5% and the maximum relative uncertainty for pressure loss coefficient $\xi$ is 4.0%.

## 4. Results and discussions

For all the test cases, the inlet temperature of kerosene is the room value and the inlet pressure changes from 2 MPa to 3 MPa. The mass flow rate is from 5 g/s to 50 g/s and the relevant Reynolds number increases from about 2020 to 14,260. Since Reynolds number of jets are larger than 2000, the jet flow is considered to be in the turbulent flow regime [20,21]. The outer surface of the target plate is heated to a wall temperature range of 380 K to 500 K determined by the mica heating facility with a temperature feedback and control system.

Repeatability of the experimental data is examined by conducting heat transfer experiments at the same flow conditions and heating power repeatedly. Table 1 presents a typical test with an inlet mass flow rate of 7 g/s and a pressure of about 3 MPa. As shown in Table 1, the difference of the pressure loss $\Delta P$ and the average heat transfer coefficient $h$ between two tests on different days are 2.94% and 3.64% respectively and a good repeatbility is confirmed.

### 4.1. Results for a typical test case

Fig. 4 (a) gives time change of inlet pressure for a typical test case with a mass flow rate of 25.2 g/s and a Reynolds number of 7440. Fig. 4 (b) shows the time change of temperature difference between the inlet and the outlet. As shown in Fig. 4, after kerosene flows into the test section with pneumatic valve opened, the pressure reaches quickly a pre-set value after a development time of about 3 s, which indicates that a steady impingement jet flow has been formed. The change of temperature difference across the test panel is found to be slower than the pressure value due to longer characteristic time of heat transfer than that of flow. As shown in Fig. 4 (b), after approximately 25 s, the temperature difference approaches a nearly constant value indicating an establishment of a steady heat transfer.

### 4.2. Results of experiments

Fig. 5 gives heat transfer coefficient and pressure loss between the inlet and the outlet as a fucntion of Reynolds number. As illustrated in Fig. 5 (a), heat transfer coefficient increases with Reynolds number, and it changes from 3650 W/(m$^2$·K) to 16,538 W/(m$^2$·K) as Reynolds number of impingement jets increases from 2020 to 14,260.

Fig. 5 (b) shows that the pressure loss increases with Reynolds number, and it changes from 6.4 kPa to 159.2 kPa. However, the maximum pressure loss is merely 7.17% of the inlet pressure value of 2 MPa, indicating a small pressure loss for kerosene impingement jet flow.

The expeirmntal data of non-dimensional heat transfer coefficient and pressure loss can be correlated as functions of Reynolds number and Prandtl number. Fig. 6 (a) gives the results of Nusselt number obtained by experiments and predicted by the correlation function as given in Eq. (5) which fits the experimantal data very well.

$$\mathrm{Nu} = 0.045\mathrm{Pr}^{0.45}\mathrm{Re}^{0.7} \tag{5}$$

As illustrated in the figure, for a Reynolds number range of 2020 to 14,260, the predicted Nusselt number agrees well with the experimental data with a maximum discrepency less than 19%. The correltion formula of Eq. (5) gives a Reynolds number power of 0.7, which is close to the power number of 0.716 for impingement jet cooling of water based on the expeirmental data of Pan et al. [22].

As illustrated in Fig. 6 (b), the non-dimensional pressure loss coefficient $\xi$ as defind by Eq. (4) is plotted. A correlation of non-dimensional pressure loss coefficient of kerosene impingement jet cooling is given as follow

$$\xi = 88\mathrm{Re}^{-0.48} \tag{6}$$

As illustrated in Fig. 6 (b), discrepency of the predicted pressure loss coefficient with the experimental data is less than 14.3% for the present Reynolds number range of 2020 to 14,260.

One can see that the pressure loss coefficient drops with Reynolds number overally. As Reynolds number is greater than 10,000, variation of the presusre loss coefficient becomes very small. This result is consistent with the conclustion obtained by the previous experimental studies of water and air flow through perforated plate [23,24]. The nearly constant value of pressure loss coefficient at high Reynolds numbers essentially has the same flow mechanism as that for discharge coefficient of flow through orifice plate since the pressure loss across the impingement jet holes contributes to the main part of the total pressure loss of the test rig. As discussed in the literature [25], discharge coefficient of water through orifice plate was measured. A similar behavior of discharge coefficient at high Reynolds numbers was found, which attributes to the effect of orfice plate on velocity profile.

## 5. Numerical results and discussions

Numerical simulation can provide details of flow and thermal fields for a better understanding of the experimental results. Reynolds Average Numerical method with SST k-ω turbulence model [26] is adopted to solve Navier-Stokes equations for simulating impingement jet flows. The SST k-ω turbulence model has been proven effective for simulation of impingement jet flows as used in the literatures [27,28]. The second-order upwind scheme is adopted for convection terms of N-S equations and the second-order central scheme is used for diffusion terms. The 10-species surrogate of kerosene [16] is used for calculation of thermal and transport properties of fuel. The surrogate model has been proven to be accurate for calculation of thermophysical and transport properties of kerosene at varied temperatures and pressures as discussed in our previous works [16].

Fig. 7 shows the computational domain and meshes for the flow region. The total mesh number is 3 million and stretched meshes are applied near the impingement surface satisfying that the dimensionless grid size from the wall, $y^+ \leq 1$ for accurate calculation of the near-wall flow properties. A no-slip wall boundary condition and a constant wall heat flux of 0.7 MW/m$^2$, which are very close to the experimental conditions, are used on the impingement surface. The other wall boundary conditions are no-slip and adiabatic. Two cases with different mass flow rate of 25 and 45 g/s are simulated.

For the purpose of validation of the present numerical method and mesh, the calculated heat transfer coefficient and pressure loss are reported in comparison with the experimental data. As illustrated in Table 2, the maximum difference of heat transfer coefficient is 10.2%, meanwhile the maximum difference of pressure loss is 11.1%. One can conclude that the numerical results are well consistent with the experimental results, and the accuracy of the adopted numerical method are validated.

Fig. 8-10 show numerical results of impingement jet flow for a kerosene mass flow rate of 25 g/s. Distribution of heat transfer coefficient on the impingement surface is shown in Fig. 8. Four kerosene jets impinge on the target plate and high values of heat transfer coefficient are observed around the stagnation point of the jets. As shown in Fig. 8, heat transfer coefficient presents a volcano-shaped distribution with

**Table 1**
Reliability of the experimental data.

| | $\dot{m}$ g/s | $T_f$ K | $P$ MPa | $\Delta P$ kPa | $h$ W/(m$^2$·K) |
|---|---|---|---|---|---|
| Test1 | 7.0 | 319.6 | 2.9 | 6.7 | 5437.8 |
| Test2 | 7.2 | 319.1 | 2.8 | 6.9 | 5243.3 |
| Deviation | 2.82% | 0.16% | 3.51% | 2.94% | 3.64% |

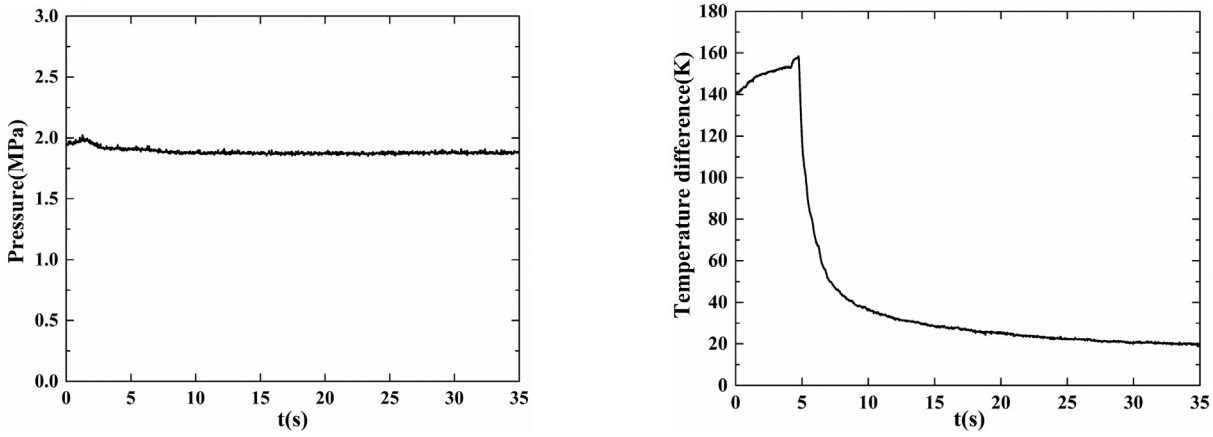


(a) Inlet pressure (b) Fuel temperature difference

**Fig. 4.** Time variations of flow parameters of kerosene.

maximum value located slightly away from the stagantion point of each jet. The shifting of the location of heat transfer peak may attribute to that the local boudary layer has a minimum thickness at the peak location as discussed in the literatures [29,30].

Contours of velocity and turbulent kinetic energy $k$ in transversal and longitudinal sections across the impingement holes are presented in Fig. 9 (a) to (d). Fig. 9 (a) and (b) present the velocity results, high speed jets are generated through the orifice plate and they impinge on the impingement surface. Thin shear layers are formed from the stagnation point of jets due to the high speed jets. The velocity shear layer would enhance flow dynamics and generate significant vortices as described in a later figure. As shown in Fig. 9 (c) and (d), large values of turbulent kinetic energy are found in the thin shear layer region, which is resulted from the impingement jets. The increase in turbulent kinetic energy is one of the major reasons for the enhanced heat transfer efficiency of impingement jet as discussed by Wan et al. for a study of air impingement jets [31].

Fig. 10 gives streamlines and iso-surfaces of $Q$ quantities of the flow field. The Q-criterion proposed by Hunt et al. [32] has been widely used to indicate vortices of flow field. The $Q$ value is defined as follows.

$$Q = \frac{1}{2}(\|\Omega\|^2 - \|S\|^2) \tag{7}$$

Where $\|\Omega\|^2$ is the rotation rate and $\|S\|^2$ is the strain rate, which are defined as $\|\Omega\|^2 = [tr(\Omega\Omega^t)]^{1/2}$ and $\|S\|^2 = [tr(SS^t)]^{1/2}$ respectively. The positive $Q$ iso-surfaces mean the areas where the strength of rotation exceeds the strain, indicating the location of strong vortices.

As shown in the Fig. 10, jet flow interacts with wall boundary layer and other jets, and counter-rotating vortices are came into being in the impinging zone. The three-dimensional vortex structures entrain fluid close to the wall into the main flow, which intensifies flow mixing and raises heat transfer efficiency significantly.

Fig. 11 (a) and (b) give distribution of heat transfer coefficient and iso-surfaces of $Q$ quantities at a higher mass flow rate of 45 g/s. As shown in the figures, the flow field and heat transfer distribution at a higher mass flow rate are quite similar to those at a lower mass flow rate of 25 g/s except that the maximum heat transfer coefficient increases from 41,980 W/(m$^2$·K) to 53,480 W/(m$^2$·K) near the stagantion points due to more intensive vortices.

## 6. Conclusions

In the current work, flow and heat transfer characteristics of impingement jets of kerosene at varied inlet flow conditions are studied experimentally and numerically. A few conclusions can be drawn from the present study.

1) The impingement jet flow of kerosene has a significant heat transfer augment. Meanwhile, the pressure loss of the impingement jet

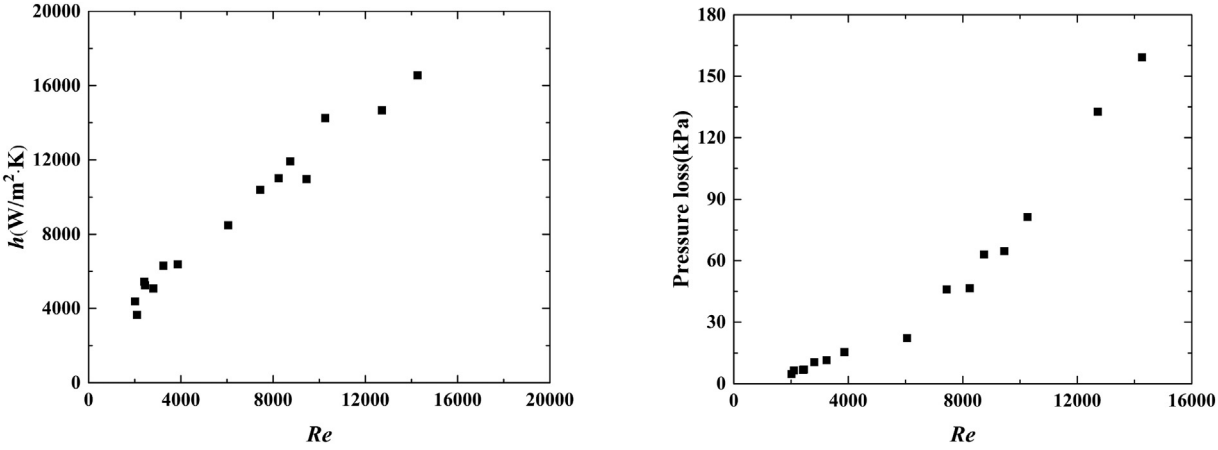


(a) Heat transfer coefficient versus $Re$ (b) Pressure loss versus $Re$

**Fig. 5.** Results of heat transfer and flow.

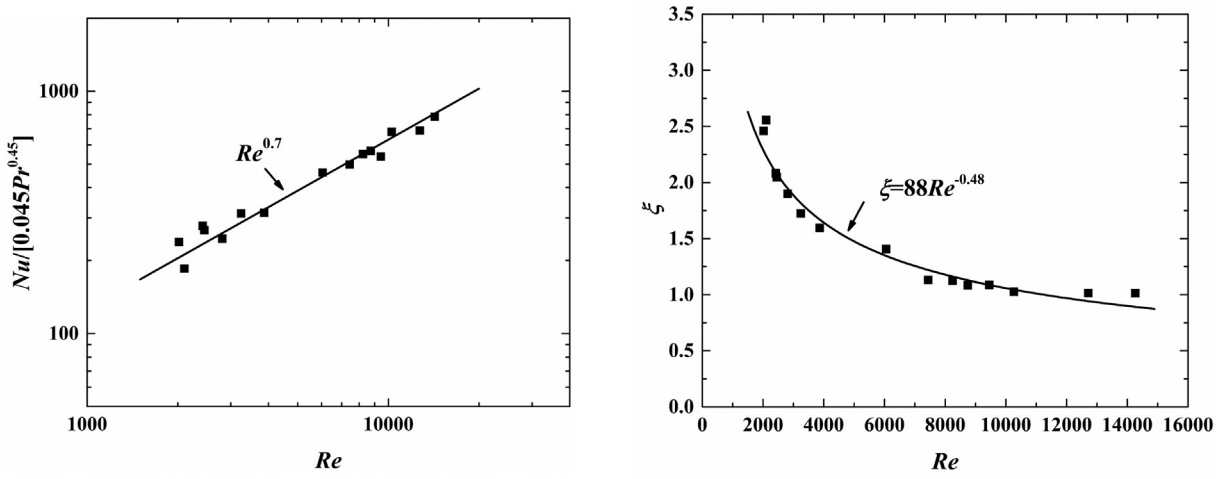


(a) *Nu* of experiments (b) Pressure loss coefficient of experiments

**Fig. 6.** Results of *Nu* and pressure loss coefficient.

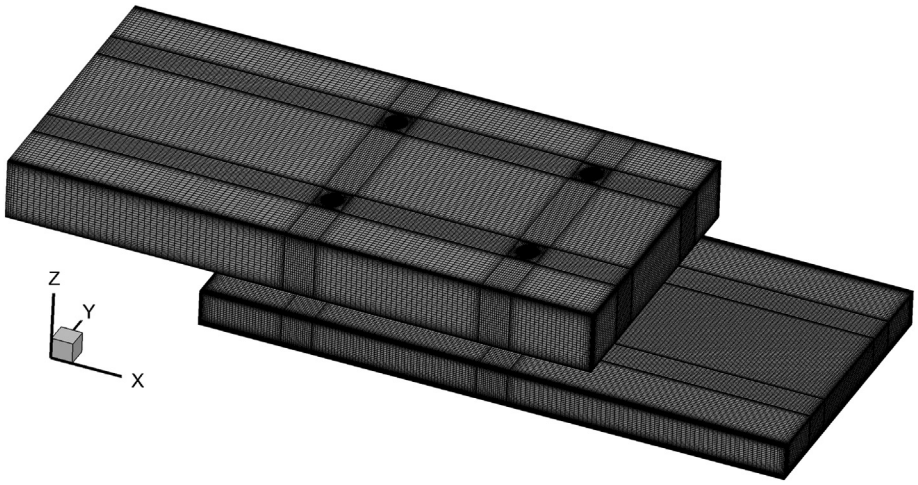


**Fig. 7.** Computational domain and Meshes for the impinging jet flow region.

**Table 2**
Comparison between experimental data and CFD results.

| Case | Results | $\dot{m}$ g/s | $h$(W/m$^2$·K) | $\Delta P$(kPa) |
|---|---|---|---|---|
| | Exp. | 25.2 | 10,381.4 | 45.9 |
| Case1 | CFD | 25.0 | 9628.7 | 40.8 |
| | Derivation | 0.79% | 7.25% | 11.11% |
| | Exp. | 44.9 | 14,664.0 | 132.6 |
| Case2 | CFD | 45.0 | 13,167.0 | 125.8 |
| | Derivation | 0.22% | 10.21% | 5.13% |

cooling structure is relatively low, accounting for less than 7.17% of the inlet fuel pressure.

2) With the increase of Reynolds number of impingement jet, the non-dimensional heat transfer coefficient, Nusselt number increases as a function of $Nu = 0.045Pr^{0.45}Re^{0.7}$ for the present impingement jet cooling configuration. The non-dimensional pressure loss coefficient decreases approximately with Reynolds number in a relation of $\xi = 88Re^{-0.48}$.

3) The present numerical results are proven accurate with comparisons to the experimental results. It is found that distribution of heat transfer coefficient on the impingement surface presents a volcano-shape with a maximum located around and slightly away the stagnation point of jets. The enhancement of heat transfer coefficient is related to the strong vortices generated by the impingement jets and the increase in turbulent kinetic energy in the boundary layer close to the impingement surface.

## Acknowledgements

This work was supported by the National Natural Science Foundation of China (Grant No. 11672307) and Youth Innovation Promotion Association, Chinese Academy of Sciences.

## CRediT author statement

**Mengmeng Du:** Writing - Original Draft, Methodology, Investigation.

**Fengquan Zhong:** Conceptualization, Methodology, Writing - Review & Editing.

**Yunfei Xing:** Investigation, Formal analysis.

**Xinyu Zhang:** Supervision.

## Declaration of Competing Interests

The authors declare that they have no known competing financial

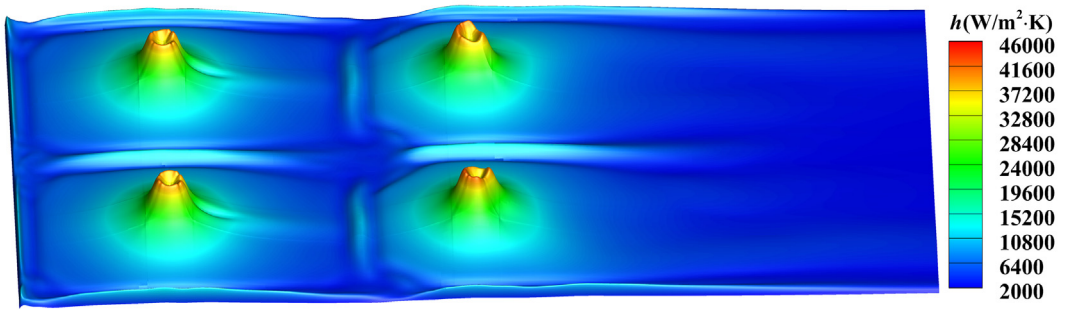


**Fig. 8.** Disrtibution of heat transfer coefficient.

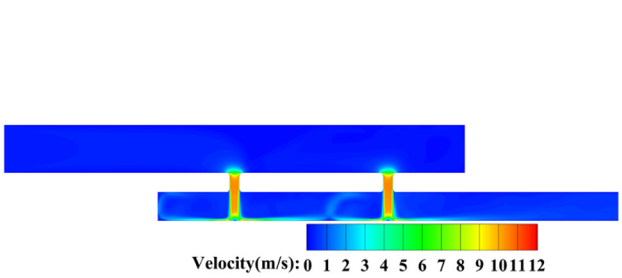


(a) Contours of velocity in a longitudinal section

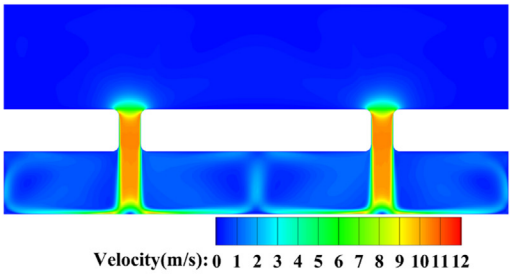


(b) Contours of velocity in a transversal section

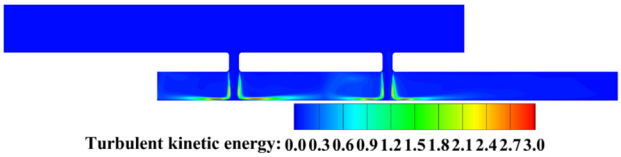


(c) Contours of turbulence kinetic energy in a longitudinal section

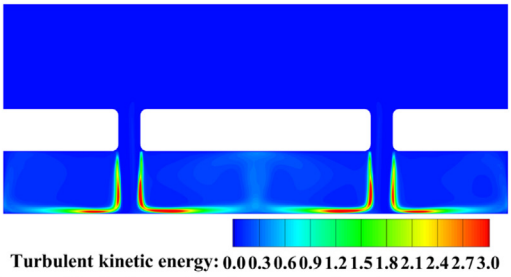


(d) Contours of turbulence kinetic energy in a transversal section

**Fig. 9.** Flow properties of impingement jet flow.

(a) Streamlines in a longitudinal section

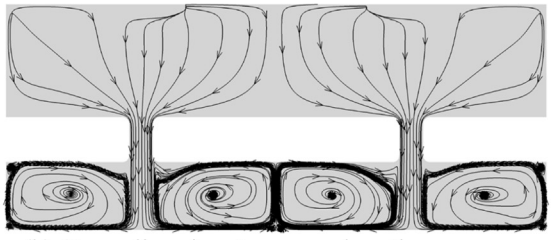

(b) Streamlines in a transversal section

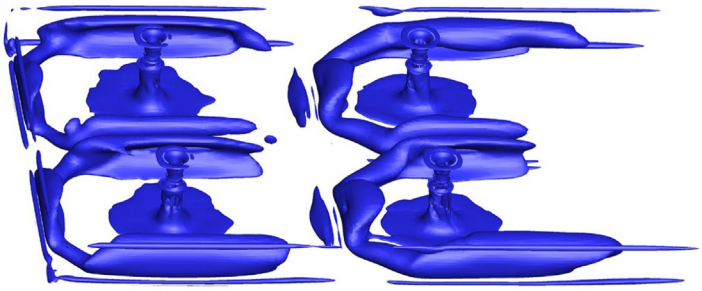

(c) Iso-surface of $Q$=1.1e6

**Fig. 10.** Flow field structure of impingement jets flow.

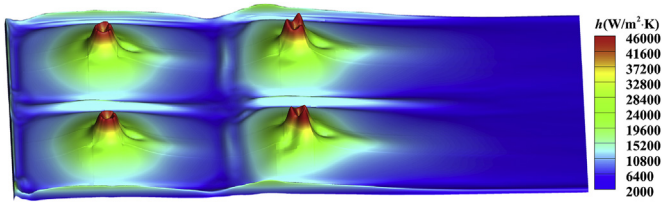


(a) Disrtibution of heat transfer coefficient

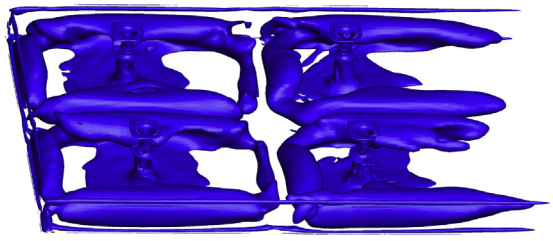

(b) Iso-surface of $Q$=1.1e6

**Fig. 11.** Heat transfer and flow properties at 45 g/s.

interests or personal relationships that could have appeared to influence the work reported in this paper.

## References


[1] M.E. Taslim, D. Bethka, Experimental and numerical impingement heat transfer in an airfoil leading-edge cooling channel with cross-flow, J. Turbomach. 131 (1) (2009) 011021–1–011021-7.

[2] S.J. Chen, A.A. Tseng, Spray and jet cooling in steel rolling, Int. J. Heat Fluid Flow 13 (4) (1992) 358–369.

[3] Y. Kondo, H. Matsushima, T. Komatsu, Optimization of pin-fin heat sinks for impingement cooling of electronic packages, J. Electron. Packag. 122 (3) (2000) 240–246.

[4] S.V. Garimella, R.A. Rice, Confined and submerged liquid jet impingement heat transfer, J. Heat Transf. 117 (4) (1995) 871–877.

[5] A.M. Huber, R. Viskanta, Effect of jet-jet spacing on convective heat-transfer to confined, impinging arrays of axisymmetric air-jets, Int. J. Heat Mass Transf. 37 (18) (1994) 2859–2869.

[6] J.Y. San, J.J. Chen, Effects of jet-to-jet spacing and jet height on heat transfer characteristics of an impinging jet array, Int. J. Heat Mass Transf. 71 (2014) 8–17.

[7] E.M. Sparrow, B.J. Lovell, Heat-transfer characteristics of an obliquely impinging circular jet, J. Heat Transf. 102 (2) (1980) 202–209.

[8] D.J. Bizzak, M.K. Chyu, Use of a laser-induced fluorescence thermal imaging-system for local jet impingement heat-transfer measurement, Int. J. Heat Mass Transf. 38 (2) (1995) 267–274.

[9] C.Y. Li, S.V. Garimella, Prandtl-number effects and generalized correlations for confined and submerged jet impingement, Int. J. Heat Mass Transf. 44 (18) (2001) 3471–3480.

[10] Y.F. Xing, S. Spring, B. Weigand, Experimental and numerical investigation of heat transfer characteristics of inline and staggered arrays of impinging jets, J. Heat Transf. 132 (9) (2010) 092201–1–092201-11.

[11] R. Yu, Jet impingement heat transfer in narrow channels with different pin fin configurations on target surfaces, J. Heat Transf. 140 (7) (2018) 072201–0722010.

[12] R. Vinzea, A. Khadea, P. Kuntikanaa, M. Ravitejb, B. Sureshb, V. Kesavanb, S.V. Prabhua, Effect of dimple pitch and depth on jet impingement heat transfer over dimpled surface impinged by multiple jets, Int. J. Therm. Sci. 145 (2019) 105974.

[13] H. Huang, L.J. Spadaccini, D.R. Sobel, Fuel-cooled thermal management for advanced aeroengines, J. Eng. Gas Turbines Power 126 (2) (2004) 284–293.

[14] D.R. Sobel, L.J. Spadaccini, Hydrocarbon fuel cooling technologies for advanced propulsion, J. Eng. Gas Turbines Power 119 (2) (1997) 344–351.

[15] V. Yang, Modeling of supercritical vaporization, mixing, and combustion processes in liquid-fueled propulsion systems, Proc. Combust. Inst. 28 (2000) 925–942.

[16] F.Q. Zhong, X.J. Fan, G. Yu, J.G. Li, C.J. Sung, Heat transfer of aviation kerosene at supercritical conditions, J. Thermophys. Heat Transf. 23 (3) (2009) 543–550.

[17] F.Q. Zhong, X.J. Fan, G. Yu, J.G. Li, C.J. Sung, Thermal cracking and heat sink capacity of aviation kerosene under supercritical conditions, J. Thermophys. Heat Transf. 25 (3) (2011) 450–456.

[18] Y.J. Zhang, F.Q. Zhong, Y.F. Xing, X.Y. Zhang, An experimental study of chilton-colburn analogy between turbulent flow and convective heat transfer of supercritical kerosene, J. Heat Transf. 139 (6) (2017) 064501–1–064501-6.

[19] S.P. Venkateshan, Mechanical Measurements, second ed., John Wiley & Sons Ltd, New York, 2015, pp. 40–42.

[20] B. Elison, B.W. Webb, Local heat-transfer to impinging liquid jets in the initially laminar, transitional, and turbulent regimes, Int. J. Heat Mass Transf. 37 (8) (1994) 1207–1216.

[21] B.W. Webb, C.F. Ma, Single phase liquid jet impingement heat transfer, Adv. Heat Tran. 26 (1995) 105–217.

[22] Y. Pan, B.W. Webb, Heat transfer characteristics of arrays of free-surface liquid jets, J. Heat Transf. 117 (4) (1995) 878–883.

[23] S. Malavasi, G. Messa, U. Fratino, A. Pagano, On the pressure losses through perforated plates, Flow Meas. Instrum. 28 (2012) 57–66.

[24] E. Ozahi, An analysis on the pressure loss through perforated plates at moderate Reynolds numbers in turbulent flow regime, Flow Meas. Instrum. 43 (2015) 6–13.

[25] H.M. Abd, O.R. Almoar, I.A. Mohamed, Effects of varying orifice diameter and Reynolds number on discharge coefficient and wall pressure, Flow Meas. Instrum. 65 (2019) 219–226.

[26] F.R. Menter, Two-equation eddy-viscosity turbulence models for engineering applications, AIAA J. 32 (8) (1994) 1598–1605.

[27] Y.Q. Zu, Y.Y. Yan, Numerical study on stagnation Point Heat Transfer by Jet Impingement in a Confined Narrow Gap, J. Heat Transf. 131 (2009) 094504–1–094504-4.

[28] B. Sagot, G. Antonini, A. Christgena, F. Buron, Jet impingement heat transfer on a flat plate at a constant wall temperature, Int. J. Therm. Sci. 47 (2008) 1610–1619.

[29] R. Gardon, J.C. Akfirat, The role of turbulence in determining the heat-transfer characteristics of impinging jets, Int. J. Heat Mass Transf. 8 (1965) 1261–1272.

[30] D.W. Colucci, R. Viskanta, Effect of nozzle geometry on local convective heat transfer to a confined impinging air jet, Exp. Thermal Fluid Sci. 13 (1996) 71–80.

[31] C.Y. Wan, Y. Rao, P. Chen, Numerical predictions of jet impingement heat transfer on square pin-fin roughened plates, Appl. Therm. Eng. 80 (2015) 301–309.

[32] J.C. Hunt, Eddies, Streams and Convergence Zones in Turbulent Flows, Proceedings of the Summer Program, Center for Turbulence Research, Stanford University, 1988, pp. 193–208.